Chemical Science

ROYAL SOCIETY OF CHEMISTRY

EDGE ARTICLE

View Article Online
View Journal | View Issue

Check for updates

Cite this: *Chem. Sci.*, 2026, **17**, 492

All publication charges for this article have been paid for by the Royal Society of Chemistry

Received 30th August 2025
Accepted 27th October 2025

DOI: 10.1039/d5sc06683b

rsc.li/chemical-science

The structural parameter of spin states of C_1-symmetric four-coordinate cobalt complexes: D_4

Chenggong Zheng, [a] Jiyong Liu, [a] Yongtao Wang, *[ac] Haoran Li, *[acd] Yuwen Wang *[b] and Zhan Lu *[ac]

Herein, we reveal the correlation between structure and spin-states for C_1-symmetric four-coordinate cobalt complexes. A series of C_1-symmetric four-coordinate cobalt complexes with various steric, electronic, anions and chelation modes were synthesized and characterized. X-ray diffraction studies revealed a structural distortion from square-planar to distorted tetrahedral pyramidal geometry. Combining paramagnetic nuclear magnetic resonance (pNMR), magnetic measurement (SQUID), X-ray photoelectron spectroscopy (XPS) and density functional theory (DFT), the electronic structure with a cobalt(II) (S_{Co} = 1/2 to 3/2) ion antiferromagnetically coupled to a radical anion ligand (S_{Ligand} = 1/2) was established. A new structural parameter, D_4, was introduced as an improved parameter for quantitatively assessing the spin state in four-coordinate complexes.

Open Access Article. Published on 03 November 2025. Downloaded on 2/10/2026 10:31:45 AM. This article is licensed under a Creative Commons Attribution-NonCommercial 3.0 Unported Licence.

Introduction

Transition metal catalysis serves as a powerful tool in organic synthesis.[1,2] Understanding structure–activity relationships remains key to developing efficient catalytic systems.[3,4] Over the past two decades, 3d transition metal catalysts have gained prominence owing to their earth abundance, favorable biocompatibility, and reduced environmental impact.[5] Nevertheless, the relationship between structure and catalytic reactivity remain elusive for these systems. This knowledge gap stems from the intrinsic challenges in characterizing 3d metal active species – their propensity for single-electron transfer processes and spin-state interconversions complicates precise determination of both oxidation and spin states during catalysis.[6–8]

Four-coordinate complexes exhibiting high reactivity have been identified as catalytically active species.[9–14] It is crucial to understand the relationship between structure and reactivity for four-coordinate complexes. For 3d metals, the fundamental insight lies in elucidating the correlation between structure and spin states. Pioneering studies by Lippard and co-workers established the relationship between the tetrahedral twist angles (Θ) and spin states in D_{2d}-symmetric M(II)–tropocoronand complexes (M = Co, Ni).[15] Smith reported the relationship between the Tolman cone angle (θ) and spin states in C_3-symmetric complexes with tris(carbene) ligands.[16] Peters described that the metal–ligand distances are strongly correlated with the spin state in C_{3v}-symmetric complexes with tris(phosphino)borate [BP_3] ligands.[17,18] Chirik reported the relationship between distorted planarity and spin states in C_{2v}-symmetric (PDI)Fe[19,20] or (PDI)Co[21] complexes (PDI = pyridinediimine). Moreover, Chirik and co-workers have also made pioneering contributions to the catalysis of C_1-symmetric four-coordinate cobalt complexes.[11,22] However, the structure–spin relationship of C_1-symmetric four-coordinate complexes has not yet been systematically investigated (Fig. 1A).

There are several challenges that need to be addressed: (1) four-coordinate complexes with fewer d-electrons are more reactive and less stable, making them more difficult to isolate and characterize. (2) The C_1-symmetric skeleton significantly increases the difficulty of obtaining X-ray diffraction structures through recrystallization. (3) The rational design of spin crossover complexes with a narrow energy window remains an elusive task.[23]

In our previous work, C_1-symmetric four-coordinate cobalt alkyl species were considered as key intermediates in various reactions including hydrogenation,[24–27] hydrosilylation,[28–30] hydroboration,[31–34] and isomerization.[35–37] However, the oxidation states, spin states, and coordination modes of these species remain elusive. Herein, we describe a series of chiral four-coordinate cobalt complexes with spin multiplicity, which display singlet to triplet transitions (Fig. 1B). Combining X-ray single-crystal diffraction, paramagnetic nuclear magnetic resonance (pNMR), and magnetic measurement (SQUID), X-ray photoelectron spectroscopy (XPS) and density functional theory (DFT), the electronic structure with a cobalt(II) ion

[a]*Department of Chemistry, Zhejiang University, Hangzhou 310058, China. E-mail: wyongtao@zju.edu.cn; lihr@zju.edu.cn; luzhan@zju.edu.cn*

[b]*Hangzhou Institute for Advanced Study, UCAS, Hangzhou 310024, China. E-mail: yuwen.wang@ucas.ac.cn*

[c]*Center of Chemistry for Frontier Technologies, ZJU-NHU United R&D Center, Zhejiang University, Hangzhou 310058, China*

[d]*College of Chemical and Biological Engineering, Zhejiang University, Hangzhou 310058, China*

© 2026 The Author(s). Published by the Royal Society of Chemistry

Open Access Article. Published on 03 November 2025. Downloaded on 2/10/2026 10:31:45 AM. This article is licensed under a Creative Commons Attribution-NonCommercial 3.0 Unported Licence.

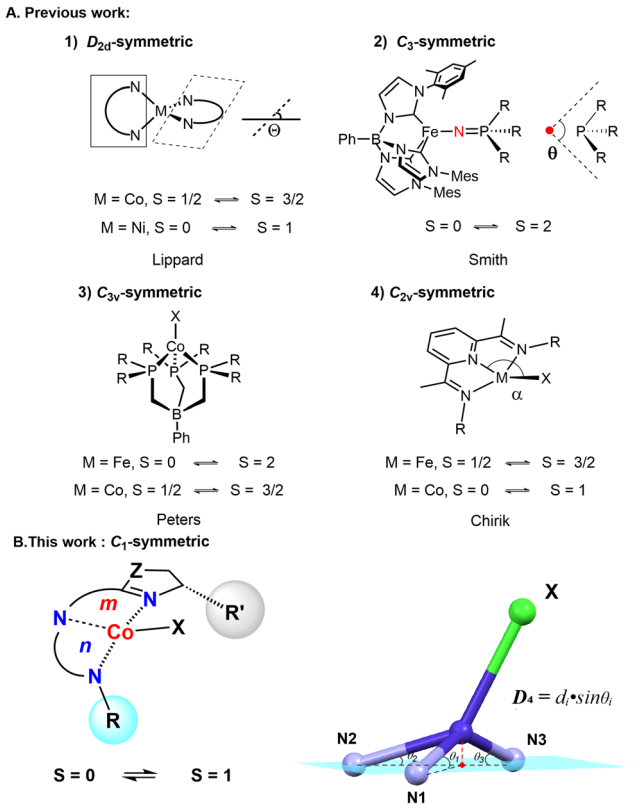

Fig. 1 (A) The relationship between structure and spin states in symmetric four-coordinate complexes. (B) The *C*1-symmetric four-coordinate complexes and structure-spin parameter, D_4.

antiferromagnetically coupled to a radical anion ligand was established. The 5,6-chelating mode plays a crucial role in modulating the spin state of the four-coordinate cobalt complexes. Furthermore, a novel structural parameter, D_4, was introduced as a metric for the spin states in four-coordinate cobalt complexes.

Results and discussion

Synthesis and characterization of cobalt complexes

In our previous work, the chiral cobalt(II) chloride complex with a 5,5-chelating oxazoline iminopyridine ligand was synthesized and characterized.[34] Inspired by the previous work, this work focuses on the synthesis of chiral cobalt methyl complex (***S***)-**L1**·$CoCH_3$, 8-oxazoline imine quinoline cobalt methyl complex (***S***)-**L2**·$CoCH_3$, 8-oxazoline iminoquinoline cobalt chloride complex (***S***)-**L2**·CoCl and 8-imidazoline iminoquinoline cobalt chloride complex (***S***)-**L3**·CoCl, following established literature procedures.[34,38] The solid-state structures of these complexes were determined using X-ray diffraction, and a representative molecular structure is illustrated in Fig. 2. Notably, although chiral oxazoline iminopyridine cobalt methyl complex (***S***)-**L1**·$CoCH_3$ has been synthesized previously,[38] to the best of our knowledge, its single-crystal structure has not been reported until now.

The representative bond distances and angles of these complexes are summarized in Table 1. The imine bonds C(2)–N(1) are measured to be 1.334(4) Å,1.317(3) Å, 1.325(5) Å and 1.336(3) Å, respectively. Compared with their precursor complexes (***S***)-**L**·$CoCl_2$, the imine bonds are elongated (Table S1). Meanwhile, the C(2)–C(3) bonds are contracted to ~1.434 Å. The variation in bond lengths within the ligands is consistent with a one-electron reduction.[39,40] That is to say, the changes in the bond distance indicate that the C_1-symmetric ligands play a non-innocent role with a radical anion chelated Co(II) metal center. Notably, the C=N double bonds of the imine are longer

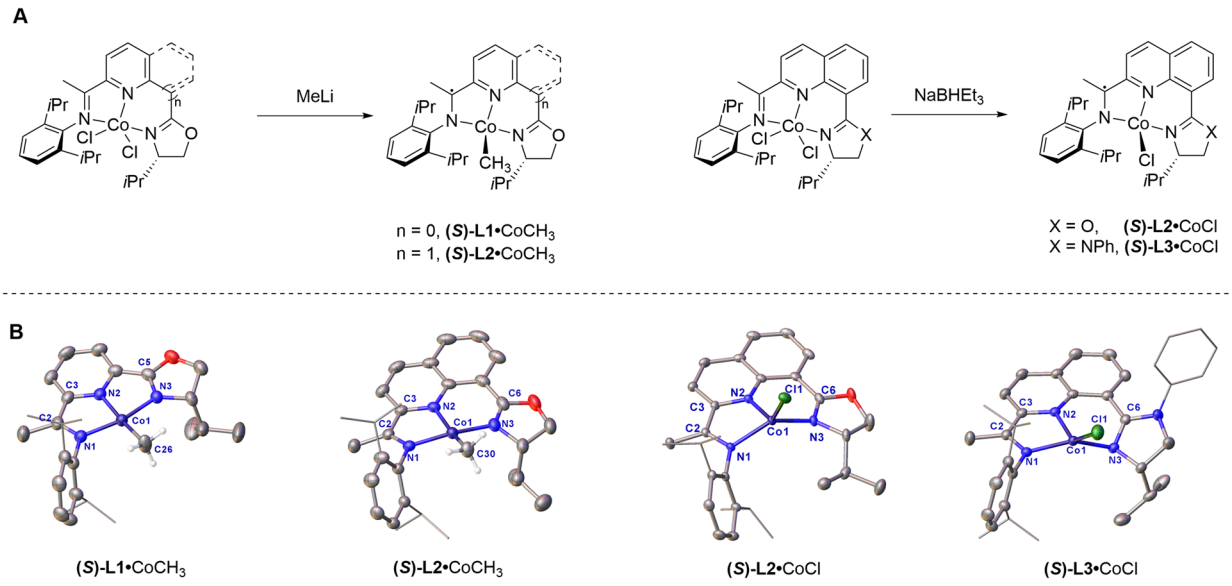

Fig. 2 (a) Synthesis of cobalt methyl complexes and cobalt chloride complexes. (b) The molecular structures of cobalt complexes depicted with 50% probability ellipsoids. All H atoms are omitted for clarity except those attached to methyl. In the unsymmetric unit cell of (***S***)-**L2**·CoCl, two distinct coordination modes coexist, *trans*- and *cis*- (Fig. S18). The *trans*- coordination mode is depicted.

© 2026 The Author(s). Published by the Royal Society of Chemistry

Open Access Article. Published on 03 November 2025. Downloaded on 2/10/2026 10:31:45 AM. This article is licensed under a Creative Commons Attribution-NonCommercial 3.0 Unported Licence.

Table 1 Comparison selected bond lengths (Å) and angles (deg) for L·$CoCH_3$ and L·CoCl

	(*S*)-**L1**·CoCl[a]	(*S*)-**L1**·$CoCH_3$	(*S*)-**L2**·$CoCH_3$	(*S*)-**L2**·CoCl[b]	(*S*)-**L3**·CoCl
C(2)–N(1)	1.329(2)	1.334(4)	1.317(3)	1.325(5)	1.336(3)
C(2)–C(3)	1.434(2)	1.432(4)	1.432(3)	1.436(5)	1.433(4)
C(5)/C(6)–N(3)[c]	1.300(2)	1.305(4)	1.288(3)	1.301(5)	1.314(3)
Co–N(1)	1.906(2)	1.887(2)	1.898(2)	1.976(3)	1.979(2)
Co–N(2)	1.811(2)	1.838(2)	1.918(2)	1.954(3)	1.957(2)
Co–N(3)	1.934(2)	1.907(2)	1.897(2)	1.984(3)	1.988(2)
Co–X	2.193(5)	1.958(3)	1.970(3)	2.259(2)	2.253(1)
N(1)–Co–N(3)	162.6(1)	162.2(1)	166.9(1)	134.8(2)	146.5(1)
N(2)–Co–X	176.3(1)	173.2(2)	164.2(1)	122.9(1)	133.6(1)
τ_4	0.15	0.18	0.20	0.73	0.57
D_4	0.037	0.057	0.206	0.744	0.568

[a] From ref. 34. [b] The bond lengths and angles were averaged over four independent molecules in the unsymmetric unit. [c] The $C_{oxazoline}$ atom on the oxazoline is labeled as C(5) in (*S*)-**L1**·$CoCH_3$ and as C(6) in (*S*)-**L2**·$CoCH_3$.

than those of oxazoline or imidazoline in four-coordinate complexes, suggesting that the imine modules play a more significant non-innocent role upon one-electron reduction of the chiral ligand.

In order to precisely quantify the geometric deviation of the cobalt center from the coordination plane, we introduce a new structural parameter, D_4, defined as the vertical distance from the metal center to the N(1)–N(2)–N(3) coordination plane (Fig. 3). The parameter can be easily calculated using Olex 2 software or other software programs.[41] The cobalt center in (*S*)-**L1**·$CoCH_3$ is nearly coplanar with the N(1)–N(2)–N(3) coordination plane, approaching an ideal square planar geometry (D_4 = 0.057 Å). This square planar configuration is consistent with the diamagnetic behavior of (*S*)-**L1**·$CoCH_3$, as observed by nuclear magnetic resonance, and indicates a strong ligand field.[13,21,42] For (*S*)-**L2**·$CoCH_3$, the geometry index (τ_4 = 0.20) is slightly larger than that of (*S*)-**L1**·$CoCH_3$ (τ_4 = 0.18),[43] while the structural parameter D_4 significantly increases to 0.206 Å. Consequently, the molecular geometry of (*S*)-**L2**·$CoCH_3$ is best described as a distorted planar structure.

Both (*S*)-**L2**·CoCl and (*S*)-**L1**·CoCl[34] are stabilized by the same coordinating atom but differ in their chelating modes. However, the subtle variation triggers dramatic differences in the coordination modes. Firstly, the X-ray analysis of (*S*)-**L2**·CoCl revealed that both *cis*- and *trans*- conformations coexist within the unsymmetric unit cell (Fig. S18). Secondly, the N(2)–Co–Cl angle is measured to be 122.9(1)° and the τ_4 index is 0.73 in (*S*)-**L2**·CoCl. The central metal atom is significantly lifted from the N(1)–N(2)–N(3) coordination plane and the D_4 value is measured to be 0.744 Å. Therefore, the molecular geometry of (*S*)-**L2**·CoCl is best described as a distorted tetrahedral structure. As for (*S*)-**L3**·CoCl, the oxazoline moiety on the ligand was replaced with a more electron-rich imidazoline group. Accordingly, the coordination structures undergo distinct modifications. In contrast to (*S*)-**L2**·CoCl, (*S*)-**L3**·CoCl presents a single *trans*-conformation. The N(2)–Co–Cl angle and τ_4 index are measured to be 133.6(1)° and 0.57, respectively. The D_4 value is measured to be 0.568 Å and is smaller than that of (*S*)-**L2**·CoCl. Correspondingly, the molecular geometry of (*S*)-**L3**·CoCl is best described as a distorted sawhorse structure.[44]

The ^{1}H NMR spectrum of the (*S*)-**L2**·$CoCH_3$ complex exhibits an interesting feature, displaying characteristics of both paramagnetic broadening (typical of paramagnetic compounds) and fine coupling splitting (typical of diamagnetic compounds) simultaneously (Fig. 4). The unique phenomenon has not been previously reported in paramagnetic cobalt complexes,[9,21,45] providing intriguing insights into the electronic structure of the complex. A solution magnetic moment of 0.77(1) μ_B was measured in benzene-d_6 at room temperature by Evans'

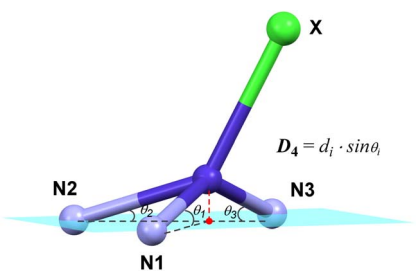

Fig. 3 Illustration of the geometric meaning of the D_4 parameter.

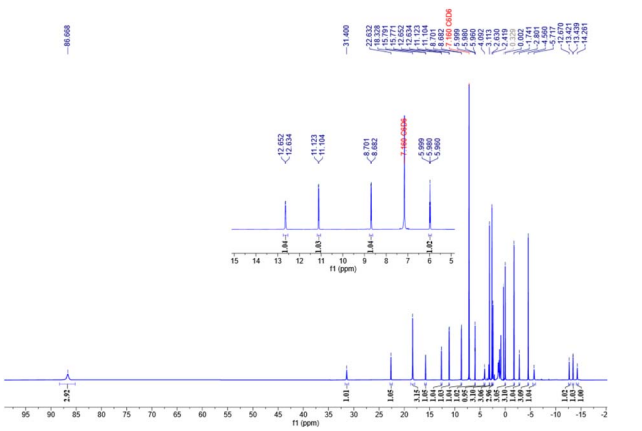

Fig. 4 ^{1}H NMR spectrum of (*S*)-**L2**·$CoCH_3$ in benzene-d_6 at 300 K.

© 2026 The Author(s). Published by the Royal Society of Chemistry

Open Access Article. Published on 03 November 2025. Downloaded on 2/10/2026 10:31:45 AM. This article is licensed under a Creative Commons Attribution-NonCommercial 3.0 Unported Licence.

method.[46] Based on the correlation between the μ_{eff} and spin state, the spin population distribution of (*S*)-**L2**·$CoCH_3$ can be described as a mixture of 93% low-spin (LS) and 7% high-spin (HS) states.[47] This indicates that (*S*)-**L2**·$CoCH_3$ exhibits mixed spin multiplicities, with contributions from both singlet and triplet states. The Gibbs energy change (ΔG) between the singlet and triplet states was calculated to be −1.4 kcal mol^{-1}.[8,48] The solution magnetic moment of (*S*)-**L2**·CoCl was measured to be 2.94(6) μ_B in benzene-d_6 at 291 K, suggesting an absolute high-spin state at this temperature. The ^{1}H NMR spectrum of the (*S*)-**L3**·CoCl complex also exhibits both paramagnetic and diamagnetic characteristics (see the SI). The solution magnetic moment of (*S*)-**L3**·CoCl was measured to be 2.59(1) μ_B in benzene-d_6 at 288 K, indicating a spin state composition of 0.16 LS + 0.84 HS. Combined analysis of X-ray diffraction and magnetic measurement reveals a clear positive correlation between an increasing population of the high-spin triplet state and a rising value of the structural parameter D_4.

The unsaturated magnetic moment of (*S*)-**L2**·$CoCH_3$ was further investigated using variable-temperature superconducting quantum interference device (SQUID) magnetometry in the solid state (Fig. 5). At approximately 2 K, the χT value of (*S*)-**L2**·$CoCH_3$ approaches zero, indicating a diamagnetic ground state with $S = 0$. Above 150 K, χT increases with temperature and does not saturate even at 350 K. The SQUID data suggest that the complex undergoes a temperature-induced spin transition from the $S = 0$ singlet state to the $S = 1$ triplet state, consistent with spin crossover behavior. The effective magnetic moment reaches 0.98 μ_B at 290 K, a value essentially consistent with that calculated by Evans' method.

X-ray photoelectron spectroscopy

XPS was performed to reveal the electronic structure and oxidation states of Co sites in the cobalt complexes. (*S*)-**L1**·$CoCl_2$, (*S*)-**L2**·$CoCl_2$ and (*S*)-**L3**·$CoCl_2$ were analyzed by XPS, affording binding energies of 781.0 eV, 780.8 eV and 780.6 eV (Fig. S15–S17). Next, (*S*)-**L1**·$CoCH_3$, (*S*)-**L2**·$CoCH_3$, (*S*)-**L2**·CoCl and (*S*)-**L3**·CoCl were carefully analyzed by XPS, affording Co $2p_{3/2}$ binding energies of 780.8 eV, 780.4 eV, 780.9 eV and 780.9 eV, respectively (Fig. 6). Their binding energies are slightly higher than that of CoO (780.0 eV),[49] supporting the +2 oxidation state of the Co species in **L**·$CoCl_2$. The binding energies of **L**·$CoCH_3$ and **L**·CoCl are similar to those of their precursor, **L**·$CoCl_2$, before reduction. The slight binding energy change further supports the ligand's redox activity, suggesting that single-electron reduction occurs on the ligand, while the oxidation state of the central metal remains constant. Combining the XRD structure, magnetic measurements, XPS analysis and DFT calculations, (*S*)-**L**·$CoCH_3$ and (*S*)-**L**·CoCl are best described as radical anions antiferromagnetically coupled to a Co(II) metal center (Fig. 8 and 9).

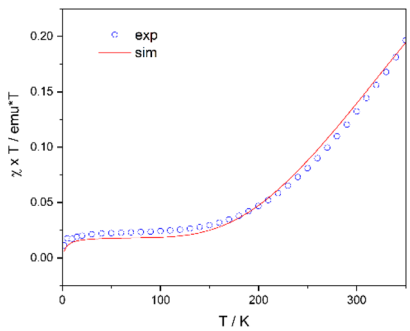

Fig. 5 Temperature dependence of magnetic susceptibility under an external magnetic field of 1 T and simulations with the domain model (solid lines) for (*S*)-**L2**·$CoCH_3$.

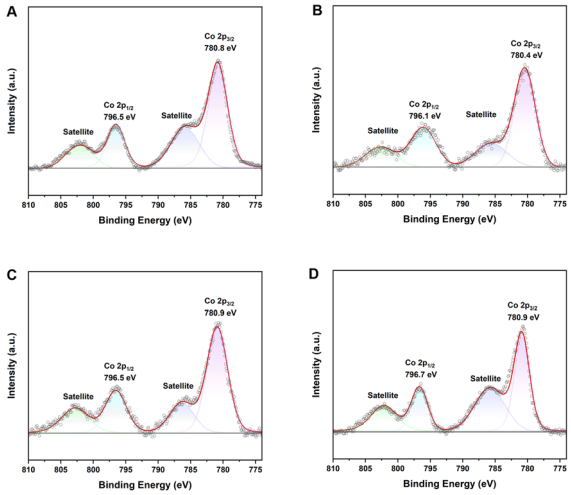

Fig. 6 XPS spectrum of Co 2p for cobalt complexes. (a) (*S*)-**L1**·$CoCH_3$; (b) (*S*)-**L2**·$CoCH_3$; (c) (*S*)-**L2**·CoCl; (d) (*S*)-**L3**·CoCl.

In order to obtain a more systematic understanding of the correlation between structure and spin states, a series of four-coordinated cobalt complexes was further synthesized and characterized (Fig. 7). The effects of steric, electronic, and anions on spin states were systematically investigated. The representative structural parameters are summarized in Table 2.

It should be noted that the geometry index τ_4 of (*S*)-**L4**·$CoCH_3$ ($\tau_4 = 0.25$) is larger than that of (*S*)-**L2**·$CoCH_3$ ($\tau_4 = 0.20$); however, (*S*)-**L4**·$CoCH_3$ exhibits diamagnetic behaviour with low-spin states. Correspondingly, the D_4 value of (*S*)-**L4**·$CoCH_3$ is measured to be 0.095 Å, which is smaller than that of (*S*)-**L2**·$CoCH_3$ ($D_4 = 0.206$ Å). Considering that the τ_4 index was initially proposed to quantify the deviation from ideal planar geometry for symmetric four-coordinate complexes, like D_{2d} and C_{2v}, the τ_4 index may not be suitable for assessing C_1-symmetric four-coordinate compounds.[43]

Comparatively, the parameter D_4 is defined geometrically as $d_i \sin\theta_i$, where d_i is the M–L bond length (reflecting ligand coordinated strength), and θ_i is the angle between the M–L bond and the coordination plane, reflecting the $d_{x^2-y^2}$ orbital overlap (Fig. 3). In other words, a smaller D_4 value is likely associated with a stronger ligand field and a larger splitting energy. Interestingly, in the UV-vis spectra, the maximum absorption wavelength of four-coordinate cobalt complexes exhibits a red shift with an increase in the D_4 value.

© 2026 The Author(s). Published by the Royal Society of Chemistry

Open Access Article. Published on 03 November 2025. Downloaded on 2/10/2026 10:31:45 AM.
This article is licensed under a Creative Commons Attribution-NonCommercial 3.0 Unported Licence.

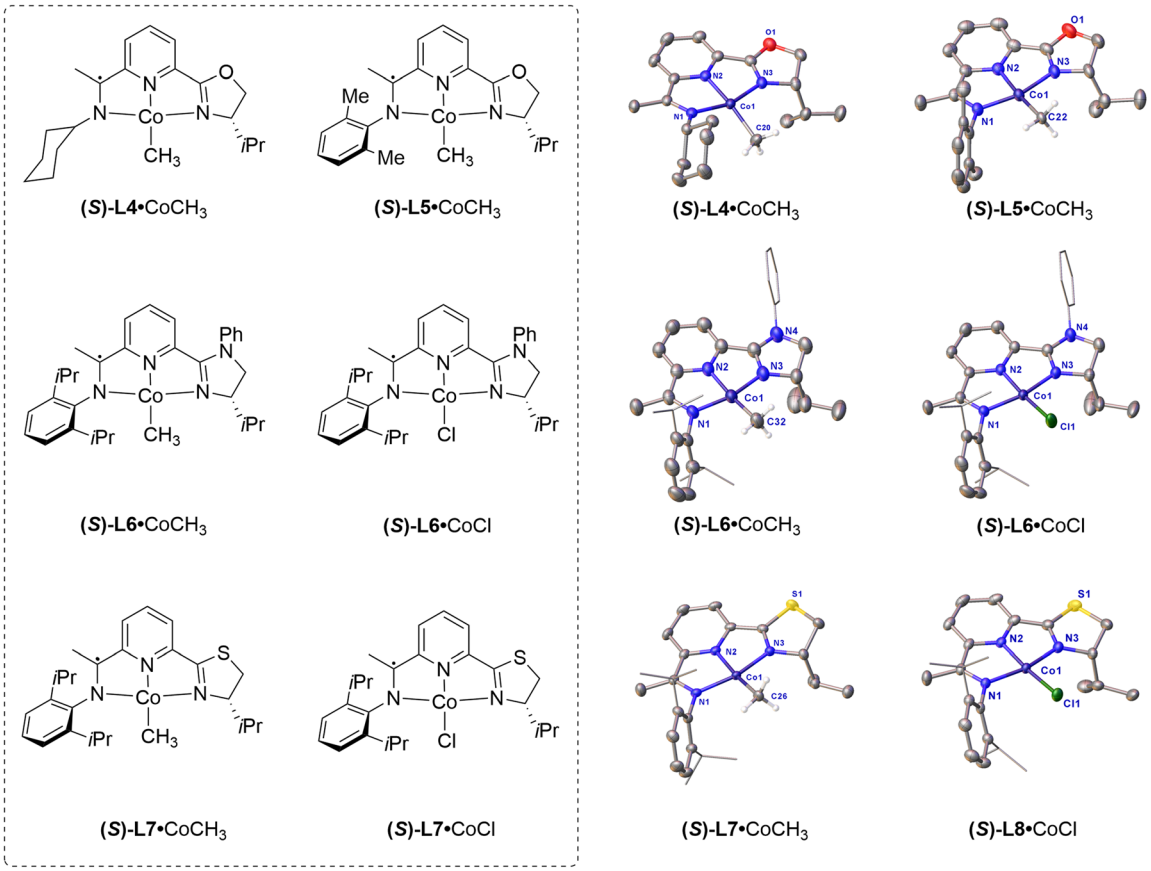

Fig. 7 Synthesis and characterization of C_1-symmetric cobalt chloride complexes and cobalt methyl complexes. The molecular structures of complexes depicted with 50% probability ellipsoids. All H atoms are emitted for clarity excepted methyl.

Computational studies

Full-molecule DFT calculations were performed on (*S*)-**L1**·$CoCH_3$ and (*S*)-**L2**·CoCl using the TPSSh[50–52] functional methods and the def2-TZVP basis set.[53–56] For (*S*)-**L1**·$CoCH_3$, the results reveal that the electronic structure adopts a broken-symmetry (BS) (1, 1) configuration,[57] with an electronic energy

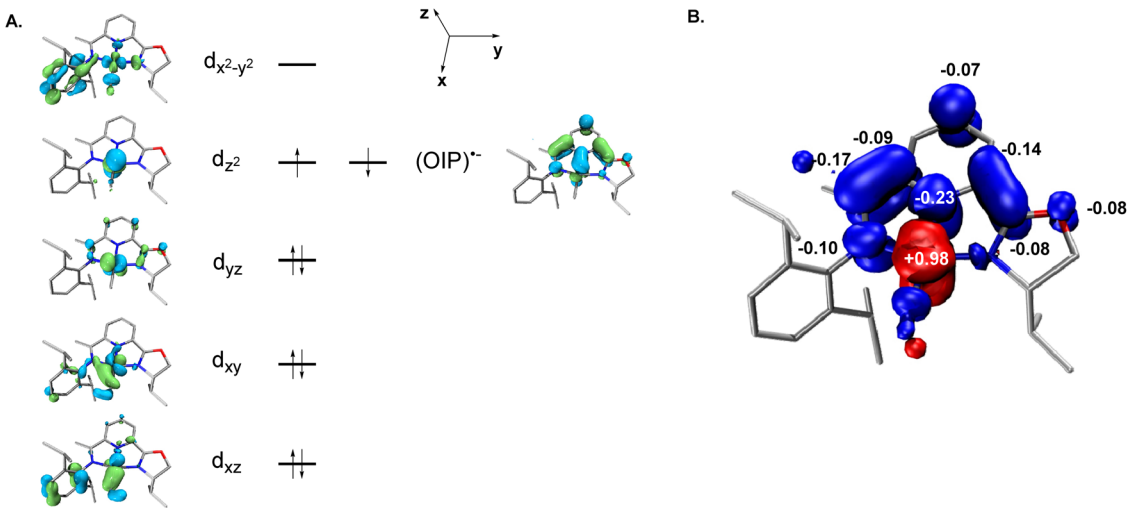

Fig. 8 (A) Qualitative molecular orbital diagram obtained from the BS(1, 1) solution for (*S*)-**L1**·$CoCH_3$ from TPSSh DFT calculations (isovalue = 0.05 a.u.). (B) The spin density plot obtained from a Muilliken population analysis of the BS(1, 1) solution for (*S*)-**L1**·$CoCH_3$ (red = positive spin density and blue = negative spin density; isovalue = 0.002 a.u.).

© 2026 The Author(s). Published by the Royal Society of Chemistry

Open Access Article. Published on 03 November 2025. Downloaded on 2/10/2026 10:31:45 AM.
This article is licensed under a Creative Commons Attribution-NonCommercial 3.0 Unported Licence.

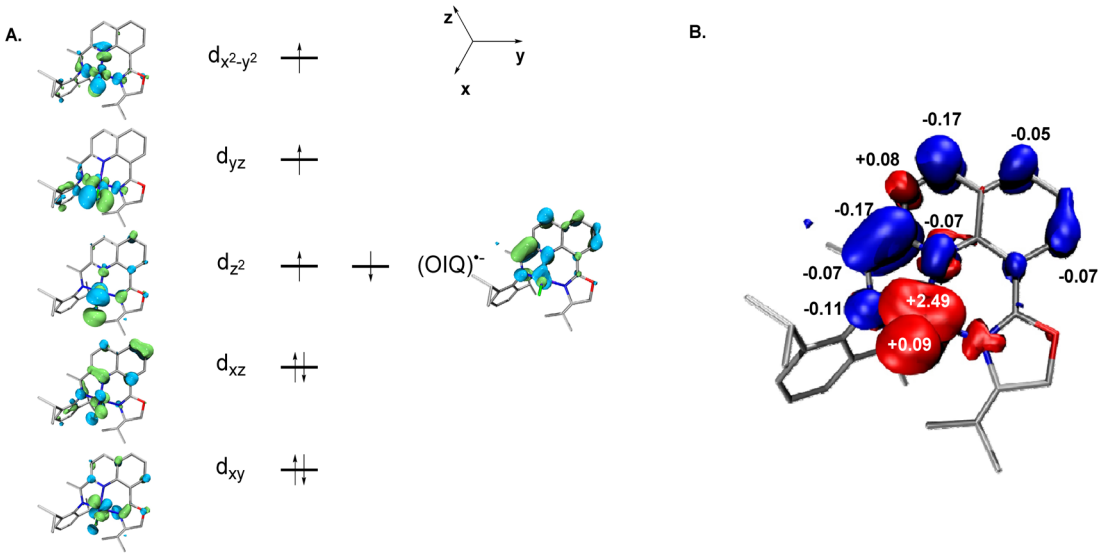

Fig. 9 (A) Qualitative molecular orbital diagram obtained from the BS(3, 1) solution for **(*S*)-L2**·CoCl from TPSSh DFT calculations (isovalue = 0.05 a.u.). (B) The spin density plot obtained from a Muilliken population analysis of the BS(3, 1) solution for **(*S*)-L2**·CoCl (red = positive spin density and blue = negative spin density; isovalue = 0.002 a.u.).

Table 2 The summary of the geometry UV-vis spectrum and the spin states of four-coordinate cobalt complexes

Complex	τ_4	D_4/Å	λ_{max}/nm	Spin states
(*S*)-L1·CoCl	0.15	0.037	515	Low spin
(*S*)-L1·$CoCH_3$	0.18	0.057	558	Low spin
(*S*)-L2·$CoCH_3$	**0.20**	**0.206**	625	0.93 LS + 0.07 HS
(*S*)-L2·CoCl	0.73	0.744	657	High spin
(*S*)-L3·CoCl	0.57	0.568	650	0.16 LS + 0.84 HS
(*S*)-L4·$CoCH_3$	**0.25**	**0.095**	545	Low spin
(*S*)-L5·$CoCH_3$	0.18	0.011	526	Low spin
(*S*)-L6·$CoCH_3$	0.16	0.045	552	Low spin
(*S*)-L6·CoCl	0.16	0.045	529	Low spin
(*S*)-L7·$CoCH_3$	0.20	0.049	577	Low spin
(*S*)-L7·CoCl	0.17	0.082	532	Low spin

−1.5 kcal mol^{-1} lower than that of the BS (3, 1) triplet state. The corresponding molecular orbital diagram and spin–density plot are illustrated in Fig. 8.[58–60] The qualitative molecular-orbital diagram is consistent with that expected for a square-planar complex with two doubly occupied cloverleaf d orbitals (d_{xy} and d_{yz}) and d_{z^2} (the *z* axis being defined as perpendicular to the chelate plane). One unpaired electron is located in the d_{xz} orbital, while the second unpaired electron occupies an oxazoline iminopyridine π* symmetry orbital. An orbital principally of $d_{x^2-y^2}$ origin is found among the unoccupied orbitals. The overall singlet ground state ($S = 0$) is confirmed by the Mulliken spin density plot, which shows antiferromagnetic coupling between a low-spin cobalt(II) ion ($S_{Co} = 1/2$) and an oxazoline iminopyridine radical anion ($S_{OIP^{\cdot-}} = 1/2$).

The **(*S*)-L2**·CoCl calculation converged to a BS (3, 1) solution, which is lower in energy by 3.7 kcal mol^{-1} than the BS (1, 1) open-shell singlet state. The corresponding molecular orbital diagram and spin–density plot are shown in Fig. 9. The qualitative molecular orbital diagram is consistent with a distorted tetrahedral complex, in which the cobalt center is significantly displaced from the coordination plane. The electronic structure of **(*S*)-L2**·CoCl is corroborated by the Mulliken spin density population analysis, confirming a high-spin cobalt(II) ion ($S_{Co} = 3/2$) antiferromagnetically coupled to an 8-oxazoline iminoquinoline radical anion ($S_{OIQ^{\cdot-}} = 1/2$), resulting in an overall $S = 1$ triplet state.

Conclusions

In summary, we reported a series of C_1-symmetric four-coordination cobalt complexes with various steric effects, electronic effects, anions and chelation modes with spin multiplicities. By modulating the chelation modes and ligand substituents, the spin states of the metal center can be effectively manipulated. The 5,6-chelating mode provides a spin-state manipulation window for four-coordination cobalt complexes. The electronic structure of the radical anion antiferromagnetically coupled Co(II) metal center was established by multiple spectra and DFT calculations. A novel structural parameter for four-coordination complexes, D_4, is proposed, which could be better correlated with the spin state of the metal center. It can be anticipated that the D_4 index could offer a predictive framework for manipulating spin and understanding the spin states of intermediates and transition states in spin chemistry.

Author contributions

Z. Lu conceived the project and supervised the work with Y. W. Wang, Y. T. Wang and H. R. Li. C. G. Zheng conducted the experiments and drafted the original manuscript. J. Y. Liu contributed to the characterization of the single crystals. Y.

Open Access Article. Published on 03 November 2025. Downloaded on 2/10/2026 10:31:45 AM. This article is licensed under a Creative Commons Attribution-NonCommercial 3.0 Unported Licence.

T. W. performed theoretical calculations. H. R. Li provided critical supervision in electronic structure analysis. Y. W. Wang provided critical guidance on the single-crystal preparation. All authors discussed the results, reviewed, and contributed to the final manuscript.

Conflicts of interest

There are no conflicts to declare.

Data availability

The data supporting this article have been included as part of the supplementary information (SI). See DOI: https://doi.org/10.1039/d5sc06683b.

CCDC 2325627, 2329552, 2338659–2338660, 2344060, 2344061, 2348647, 2353792, 2355865, 2355871, 2356769, 2362794, 2369004, 2375363, 2375454, 2374877 and 2475931 ((*S*)-**L**·$CoCl_2$, (*S*)-**L**·$CoCH_3$ and (*S*)-**L**·CoCl) contain the supplementary crystallographic data for this paper.[61a–q]

Acknowledgements

Financial support was provided by the National Key R&D Program of China (2021YFF0701600), the Zhejiang Provincial Natural Science Foundation of China (LDQ24B020001), the National Natural Science Foundation of China (NSFC) (22525109), the Fundamental Research Funds for the Central Universities (226-2022-00224 and 226-2024-00003), the Strategic Priority Research Program of the Chinese Academy of Sciences (Grant No. XDB0610000), and the Research Funds of the Hangzhou Institute for Advanced Study, UCAS (Grant No. 2024HIAS-p003). We thank Wang Chen and Prof. Shengfa Ye from the Dalian Institute of Chemical Physics for SQUID analysis and helpful discussions. We thank Dr Xiang Ren for providing help in synthesizing 8-OIQ ligands. We thank Prof. Qiaohong He for ESI-HRMS analysis. We thank Dr Dier Shi, Shuna Liu, Minghang Li and Jinyi Li for XPS analysis. We thank Dr Hongliang Wang and Peihong Zhou for helpful computational suggestions. We thank Jialian Ding for UV-vis analysis. The authors also thank Lixuan Zheng, Jiale Ying, Zhanchen Ye, Prof. Jianguo Huang and Prof. Longguan Zhu for their helpful discussions.

Notes and references

1 A. H. Cherney, N. T. Kadunce and S. E. Reisman, *Chem. Rev.*, 2015, **115**, 9587–9652.
2 H. Wang, J. Wen and X. Zhang, *Chem. Rev.*, 2021, **121**, 7530–7567.
3 J. F. Hartwig, *Organotransition Metal Chemistry*, University Science Books, Sausalito, CA, 2010.
4 H. R. Crabtree, *The Organometallic Chemistry of the Transition Metals*, Wiley-Interscience, New York, 6th edn, 2014.
5 J. Guo, Z. Cheng, J. Chen, X. Chen and Z. Lu, *Acc. Chem. Res.*, 2021, **54**, 2701–2716.
6 M. Swart and M. Gruden, *Acc. Chem. Res.*, 2016, **49**, 2690–2697.
7 K. D. Vogiatzis, M. V. Polynski, J. K. Kirkland, J. Townsend, A. Hashemi, C. Liu and E. A. Pidko, *Chem. Rev.*, 2019, **119**, 2453–2523.
8 J. Cirera, M. Via-Nadal and E. Ruiz, *Inorg. Chem.*, 2018, **57**, 14097–14105.
9 J. V. Obligacion, S. P. Semproni and P. J. Chirik, *J. Am. Chem. Soc.*, 2014, **136**, 4133–4136.
10 J. M. Hoyt, V. A. Schmidt, A. M. Tondreau and P. J. Chirik, *Science*, 2015, **349**, 960–963.
11 M. R. Friedfeld, M. Shevlin, G. W. Margulieux, L. C. Campeau and P. J. Chirik, *J. Am. Chem. Soc.*, 2016, **138**, 3314–3324.
12 C. K. Blasius, V. Vasilenko, R. Matveeva, H. Wadepohl and L. H. Gade, *Angew. Chem., Int. Ed.*, 2020, **59**, 23010–23014.
13 J. S. Doll, M. L. Heldner, M. Scherr, J. Ballmann and D.-A. Roşca, *ACS Catal.*, 2023, **13**, 8770–8782.
14 K. E. Berger, R. J. Martinez, J. Zhou and C. Uyeda, *J. Am. Chem. Soc.*, 2023, **145**, 9441–9447.
15 B. S. Jaynes, L. H. Doerrer, S. Liu and S. J. Lippard, *Inorg. Chem.*, 1995, **34**, 5735–5744.
16 H.-J. Lin, D. Siretanu, D. A. Dickie, D. Subedi, J. J. Scepaniak, D. Mitcov, R. Clérac and J. M. Smith, *J. Am. Chem. Soc.*, 2014, **136**, 13326–13332.
17 D. M. Jenkins and J. C. Peters, *J. Am. Chem. Soc.*, 2005, **127**, 7148–7165.
18 S. E. Creutz and J. C. Peters, *Inorg. Chem.*, 2016, **55**, 3894–3906.
19 A. C. Bowman, C. Milsmann, E. Bill, Z. R. Turner, E. Lobkovsky, S. DeBeer, K. Wieghardt and P. J. Chirik, *J. Am. Chem. Soc.*, 2011, **133**, 17353–17369.
20 C. B. Kovel, J. M. Darmon, S. C. E. Stieber, G. Pombar, T. P. Pabst, B. Theis, Z. R. Turner, O. Ungor, M. Shatruk, S. DeBeer and P. J. Chirik, *J. Am. Chem. Soc.*, 2023, **145**, 5061–5073.
21 A. C. Bowman, C. Milsmann, E. Bill, E. Lobkovsky, T. Weyhermuller, K. Wieghardt and P. J. Chirik, *Inorg. Chem.*, 2010, **49**, 6110–6123.
22 S. Monfette, Z. R. Turner, S. P. Semproni and P. J. Chirik, *J. Am. Chem. Soc.*, 2012, **134**, 4561–4564.
23 S. Ye and F. Neese, *Inorg. Chem.*, 2010, **49**, 772–774.
24 J. Chen, C. Chen, C. Ji and Z. Lu, *Org. Lett.*, 2016, **18**, 1594–1597.
25 J. Guo, B. Cheng, X. Shen and Z. Lu, *J. Am. Chem. Soc.*, 2017, **139**, 15316–15319.
26 J. Guo, X. Shen and Z. Lu, *Angew. Chem., Int. Ed.*, 2017, **56**, 615–618.
27 P. Lu, H. Wang, Y. Mao, X. Hong and Z. Lu, *J. Am. Chem. Soc.*, 2022, **144**, 17359–17364.
28 B. Cheng, P. Lu, H. Zhang, X. Cheng and Z. Lu, *J. Am. Chem. Soc.*, 2017, **139**, 9439–9442.
29 J. Guo, H. L. Wang, S. P. Xing, X. Hong and Z. Lu, *Chem*, 2019, **5**, 881–895.
30 Z. Cheng, M. Li, X. Y. Zhang, Y. Sun, Q. L. Yu, X. H. Zhang and Z. Lu, *Angew. Chem., Int. Ed.*, 2023, **62**, e202215029.

© 2026 The Author(s). Published by the Royal Society of Chemistry

Open Access Article. Published on 03 November 2025. Downloaded on 2/10/2026 10:31:45 AM. This article is licensed under a Creative Commons Attribution-NonCommercial 3.0 Unported Licence.

31 J. H. Chen, T. Xi, X. Ren, B. Cheng, J. Guo and Z. Lu, *Org. Chem. Front.*, 2014, **1**, 1306–1309.
32 X. Ren and Z. Lu, *Org. Lett.*, 2021, **23**, 8370–8374.
33 C. Chen, H. Wang, T. Li, D. Lu, J. Li, X. Zhang, X. Hong and Z. Lu, *Angew. Chem., Int. Ed.*, 2022, **61**, e202205619.
34 Y. Bao, C. Zheng, K. Xiong, C. Hu, P. Lu, Y. Wang and Z. Lu, *J. Am. Chem. Soc.*, 2024, **146**, 21089–21098.
35 J. Zhao, B. Cheng, C. Chen and Z. Lu, *Org. Lett.*, 2020, **22**, 837–841.
36 W. Liu, Y. Zheng, Y. Mao, J. Chen, X. Ren, Z. Cheng and Z. Lu, *Org. Lett.*, 2022, **24**, 1158–1163.
37 J. Zhao, G. Xu, X. Wang, J. Liu, X. Ren, X. Hong and Z. Lu, *Org. Lett.*, 2022, **24**, 4592–4597.
38 L. Zhang, Z. Zuo, X. Wan and Z. Huang, *J. Am. Chem. Soc.*, 2014, **136**, 15501–15504.
39 Q. Knijnenburg, D. Hetterscheid, T. M. Kooistra and P. H. M. Budzelaar, *Eur. J. Inorg. Chem.*, 2004, **2004**, 1204–1211.
40 A. C. Bowman, C. Milsmann, C. C. Atienza, E. Lobkovsky, K. Wieghardt and P. J. Chirik, *J. Am. Chem. Soc.*, 2010, **132**, 1676–1684.
41 **https://www.bilibili.com/video/BV15y4y1773o/?spm_id_from=333.337.search-card.all.click&vd_source=0362e9aeb0256418dc579a053f424d21**.
42 J. Lee, D. Heo, W. Lee and J. Seo, *J. Am. Chem. Soc.*, 2025, **147**, 14997–15005.
43 L. Yang, D. R. Powell and R. P. Houser, *Dalton Trans.*, 2007, **9**, 955–964.
44 M. H. Reineke, M. D. Sampson, A. L. Rheingold and C. P. Kubiak, *Inorg. Chem.*, 2015, **54**, 3211–3217.
45 C. Chen, T. R. Dugan, W. W. Brennessel, D. J. Weix and P. L. Holland, *J. Am. Chem. Soc.*, 2014, **136**, 945–955.
46 S. K. Sur, *J. Magn. Reson.*, 1989, **82**, 169–173.
47 K. Sun, Y. Huang, Q. Wang, W. Zhao, X. Zheng, J. Jiang and H. L. Jiang, *J. Am. Chem. Soc.*, 2024, **146**, 3241–3249.
48 F. Milocco, F. de Vries, I. M. A. Bartels, R. W. A. Havenith, J. Cirera, S. Demeshko, F. Meyer and E. Otten, *J. Am. Chem. Soc.*, 2020, **142**, 20170–20181.
49 M. C. Biesinger, B. P. Payne, A. P. Grosvenor, L. W. M. Lau, A. R. Gerson and R. S. Smart, *Appl. Surf. Sci.*, 2011, **257**, 2717–2730.
50 V. N. Staroverov, G. E. Scuseria, J. M. Tao and J. P. Perdew, *J. Chem. Phys.*, 2003, **119**, 12129–12137.
51 J. Tao, J. P. Perdew, V. N. Staroverov and G. E. Scuseria, *Phys. Rev. Lett.*, 2003, **91**, 146401.
52 V. N. Staroverov, G. E. Scuseria, J. Tao and J. P. Perdew, *J. Chem. Phys.*, 2004, **121**, 11507.
53 A. Schäfer, C. Huber and R. Ahlrichs, *J. Chem. Phys.*, 1994, **100**, 5829–5835.
54 K. Eichkorn, F. Weigend, O. Treutler and R. Ahlrichs, *Theor. Chem. Acc.*, 1997, **97**, 119–124.
55 F. Weigend and R. Ahlrichs, *Phys. Chem. Chem. Phys.*, 2005, **7**, 3297–3305.
56 F. Weigend, *Phys. Chem. Chem. Phys.*, 2006, **8**, 1057–1065.
57 F. Neese, *J. Phys. Chem. Solids*, 2004, **65**, 781–785.
58 T. Lu and F. Chen, *J. Comput. Chem.*, 2012, **33**, 580–592.
59 T. Lu, *J. Chem. Phys.*, 2024, **161**, 082503.
60 W. Humphrey, A. Dalke and K. Schulten, *J. Mol. Graphics*, 1996, **14**, 33–38.
61 (*a*) CCDC 2325627: Experimental Crystal Structure Determination, 2025, DOI: **10.5517/ccdc.csd.cc2j207w**; (*b*) CCDC 2329552: Experimental Crystal Structure Determination, 2025, DOI: **10.5517/ccdc.csd.cc2j62vp**; (*c*) CCDC 2338659: Experimental Crystal Structure Determination, 2025, DOI: **10.5517/ccdc.csd.cc2jhkm7**; (*d*) CCDC 2338660: Experimental Crystal Structure Determination, 2025, DOI: **10.5517/ccdc.csd.cc2jhkn8**; (*e*) CCDC 2344060: Experimental Crystal Structure Determination, 2025, DOI: **10.5517/ccdc.csd.cc2jp5v8**; (*f*) CCDC 2344061: Experimental Crystal Structure Determination, 2025, DOI: **10.5517/ccdc.csd.cc2jp5w9**; (*g*) CCDC 2348647: Experimental Crystal Structure Determination, 2025, DOI: **10.5517/ccdc.csd.cc2jtyt4**; (*h*) CCDC 2353792: Experimental Crystal Structure Determination, 2025, DOI: **10.5517/ccdc.csd.cc2k09sp**; (*i*) CCDC 2355871: Experimental Crystal Structure Determination, 2025, DOI: **10.5517/ccdc.csd.cc2k0dbb**; (*j*) CCDC 2355865: Experimental Crystal Structure Determination, 2025, DOI: **10.5517/ccdc.csd.cc2k2gns**; (*k*) CCDC 2356769: Experimental Crystal Structure Determination, 2025, DOI: **10.5517/ccdc.csd.cc2k3dtx**; (*l*) CCDC 2362794: Experimental Crystal Structure Determination, 2025, DOI: **10.5517/ccdc.csd.cc2k9p5r**; (*m*) CCDC 2369004: Experimental Crystal Structure Determination, 2025, DOI: **10.5517/ccdc.csd.cc2kj4hr**; (*n*) CCDC 2374877: Experimental Crystal Structure Determination, 2025, DOI: **10.5517/ccdc.csd.cc2kq7yh**; (*o*) CCDC 2375363: Experimental Crystal Structure Determination, 2025, DOI: **10.5517/ccdc.csd.cc2kqrmp**; (*p*) CCDC 2375454: Experimental Crystal Structure Determination, 2025, DOI: **10.5517/ccdc.csd.cc2kqvkq**; (*q*) CCDC 2475931: Experimental Crystal Structure Determination, 2025, DOI: **10.5517/ccdc.csd.cc2p3drz**.

© 2026 The Author(s). Published by the Royal Society of Chemistry